

## Space Weather

### RESEARCH ARTICLE

10.1029/2018SW001921

#### Special Section:

Space Weather Events of 4–10  
September 2017

#### Key Points:

- In September 2017 a solar particle event was recorded as GLE by neutron monitors and also measured by several space-borne detectors
- Proton spectra during the event are derived from GOES data and validated through comparison to neutron monitor measurements
- Dose rates are derived for different exposure scenarios in space and aviation. The results are compared to measurements, where available

#### Supporting Information:

- Supporting Information S1
- Figure S1

#### Correspondence to:

D. Matthiä,  
daniel.matthiae@dlr.de

#### Citation:



Matthiä, D., Meier, M. M., & Berger, T. (2018). The solar particle event on 10–13 September 2017: Spectral reconstruction and calculation of the radiation exposure in aviation and space. *Space Weather*, 16. <https://doi.org/10.1029/2018SW001921>

Received 27 APR 2018

Accepted 9 JUL 2018

Accepted article online 17 JUL 2018

## The Solar Particle Event on 10–13 September 2017: Spectral Reconstruction and Calculation of the Radiation Exposure in Aviation and Space

Daniel Matthiä<sup>1</sup> , Matthias M. Meier<sup>1</sup> , and Thomas Berger<sup>1</sup> 

<sup>1</sup>German Aerospace Center (DLR), Institute of Aerospace Medicine, Cologne, Germany

**Abstract** The solar energetic particle event on 10 September 2017 and on the following days was the strongest event in recent years. It was recorded as ground level enhancement 72 by neutron monitor stations on Earth and measured by a number of instruments in space. One aspect of such a space weather event is the potentially increased radiation exposure in aviation and space. Numerical simulations can help estimate the elevated dose rates during such an event; a critical aspect in these simulations is the description of the primary particle spectrum. In this work, we present 1-hr averaged proton spectra during the event derived from Geostationary Operational Environmental Satellite measurements and described by two different analytic functions. The derived proton spectra are used to calculate the radiation exposure in aviation and different space scenarios: low-Earth orbit, interplanetary space, and Mars surface, and the results are discussed in the context of available experimental data. While the results indicate that in most of these scenarios in aviation and space the event was of little significance compared to the total exposure from galactic cosmic radiation, the skin dose in a lightly shielded environment in interplanetary space may have reached about 30% to 60% of the NASA 30-day dose limit.

### 1. Introduction

Solar energetic particles (SEP) are considered a major threat for human space exploration potentially harming both the health of the astronauts and electronics of spacecraft. The additional exposure from energetic particles can also be of concern for astronauts in low-Earth orbit onboard the International Space Station (ISS) and for airline personnel on high-altitude and high-latitude flights. One of the strongest SEP events of recent years occurred between 10 and 13 September 2017. At a time of unprecedented coverage of radiation monitors, this event offers the opportunity to study its relevance in terms of exposure at locations which are of present relevance to mankind, that is, at aviation altitudes and the ISS, and locations which will become relevant in the near future, that is, during a transit to moon, in lunar orbit, on the lunar surface, and in the mid-term future on the Martian surface.

The energetic particles originated from a solar X-ray flare (X8.2 on the NOAA scale) at the NOAA active region 12673 and from the subsequent coronal mass ejection (CME). This region had already produced several X-ray flares and an SEP event starting 4 September 2017 (Figure 1; for a comprehensive overview of the events see Redmon et al., 2018). Following an M5.5-class flare on 4 September, protons with energies mostly below 30–50 MeV were produced. Another two larger X-ray flares occurred even before the small Forbush decrease in galactic cosmic radiation (GCR) intensity related to the first event was recorded by neutron monitor stations at around 00:00 UTC on 7 September 2017. The second event showed a much stronger response in neutron monitors leading to a Forbush decrease in count rates of more than 5% starting on 8 September 2017. During the recovery phase of the Forbush decrease, AR12673 erupted again with an X9.3 (GOES-15) class flare. The Geostationary Operational Environmental Satellite (GOES) measured X-ray flux started to increase at around 15:50 UTC on 10 September 2017; the flux of highly energetic protons followed about 10 min later. At the same time the Fort Smith (FSMT) station, located in the Northwest Territories in Canada at (60.02°N, 111.93°W) and an altitude of 180 m above sea level, was the first neutron monitor to record increased count rates. Furthermore, the increase in cosmic ray intensities was measured by several other neutron monitor stations some 30 min later at around 16:30 UTC (Figure 1c).

The increase in neutron monitor count rates is a clear indication that during the event protons were accelerated to energies above several hundred MeV in relevant numbers. Whether such an event is accompanied

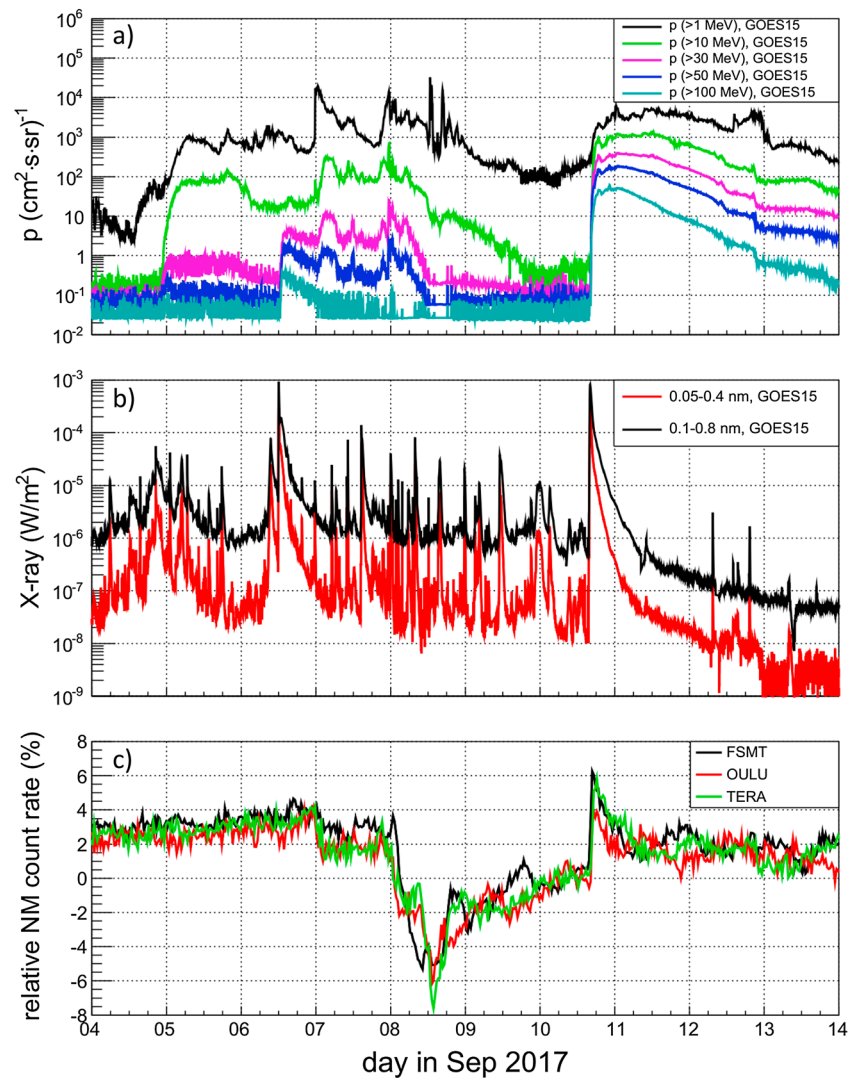


**Figure 1.** Overview of the period of increased solar activity in September 2017: (a) integral proton flux measured by Geostationary Operational Environmental Satellite-15 (GOES-15); (b) X-ray intensity measured by GOES-15; (c) neutron monitor count rates relative to the preground-level enhanced measurements on 10 September 2017 (Fort Smith-FSMT at 60.02°N, 111.93°W; Oulu-OULU at 65.05°N, 25.47°E; Terre Adelie-TERA at 66.65°S, 140°E).

with a relevant increase in radiation exposure from cosmic particles or not depends on the specific conditions. Magnetic, atmospheric, and mass shielding differ from one situation to the other:

1. Aircraft flying at low altitudes and low latitudes are well protected by either the Earth's magnetic field or the atmosphere and may not experience a significant increase. The situation may be different at high altitudes and high latitudes where the atmospheric and magnetic shielding is reduced.
2. The ISS is in an orbit in which it is most of the time well protected from protons up to several hundred MeV by the Earth's magnetic field. Only at high latitudes in a limited range of longitudes is the magnetic shielding reduced to a level that energetic protons below a few hundred MeV can reach the station. ISS itself additionally provides a significant amount of mass shielding. The amount of shielding can differ significantly at different locations inside the station. Jadrníčková et al. (2009) give average values between 30 and 50  $\text{g/cm}^2$  for different modules. The average shielding for the COLUMBUS module estimated from a CAD model and used in Berger et al. (2018) is 50  $\text{g/cm}^2$ .
3. In interplanetary space, spacecraft and space suits are the only protection for astronauts providing mass shielding.

4. Mars has only an insignificant localized magnetic field but a thin atmosphere that provides mass shielding for astronauts on the surface in future exploration missions.

In this work the relevant SEP proton spectra during the event are derived from GOES measurements. The results can be applied to any of the above mentioned scenarios to investigate the effect of an event similar to the September 2017 event on the radiation exposure. A selection of calculation of dose rates and event dose rates for the aviation and space scenarios are presented.

## 2. Reconstruction of Energetic Proton Spectra

Measurements of the Electron, Proton and Alpha Detector (EPEAD) and the High-Energy Proton and Alpha Detector (HEPAD) instruments onboard GOES-15 (Rodriguez et al., 2014) were used to reconstruct the differential energy spectra during the event. The calibration of the GOES energy channels provided by Bruno (2017) was applied. The recorded GOES data were averaged over 1-hr periods starting on 10 September 2017 16:30 UTC until 12 September 2017 22:30 UTC, which corresponds to 54 time intervals. Two different analytic functions were used to describe the primary proton spectra during the event. The first is a single power law in rigidity  $R$  for the differential particle flux  $j$  (particles/area/time/solid angle/energy). The rigidity is defined as the particle's momentum divided by its charge and is a measure for its ability to penetrate a magnetic field.

$$j(R) = J_0 \cdot (R / (\text{GV} \cdot c^{-1}))^{-\gamma} \quad (1)$$

$c$  is the speed of light.  $\gamma$  is the spectral index, and  $J_0$  is the differential flux at  $R = 1 \text{ GV}/c$ .

The second function is a combination of two power law spectra that describes the integral rigidity spectrum and that was introduced by Band et al. (1993) and successfully applied to a number of GLEs by Tylka and Dietrich (2009) and Tylka et al. (2010). Here  $J(>R)$  is the integral flux of particles with rigidities greater than  $R$  (i.e.,  $J$  = particles/area/time/solid angle).

$$\begin{aligned} J(>R) &= J_0 \cdot \left( \frac{R}{\text{GV} \cdot c^{-1}} \right)^{-\tilde{\gamma}_1} \exp\left( -\frac{R}{R_0} \right) & \text{for } R \leq (\tilde{\gamma}_2 - \tilde{\gamma}_1) R_0 \\ J(>R) &= J_0 \cdot \left( \frac{R}{\text{GV} \cdot c^{-1}} \right)^{-\tilde{\gamma}_2} \left( \frac{(\tilde{\gamma}_2 - \tilde{\gamma}_1) R_0}{\text{GV} \cdot c^{-1}} \right)^{(\tilde{\gamma}_2 - \tilde{\gamma}_1)} \exp(\tilde{\gamma}_2 - \tilde{\gamma}_1) & \text{for } R > (\tilde{\gamma}_2 - \tilde{\gamma}_1) R_0 \end{aligned} \quad (2)$$

The Band function in equation (2) approximates power laws in rigidity both in the low rigidity region with a spectral index  $\tilde{\gamma}_1$  and in the high rigidity region with a spectral index  $\tilde{\gamma}_2$ . The transition region between the two power laws is quantified by the parameter  $R_0$ . In order to directly compare the two functions, the derivative of equation (2) with respect to  $R$  was taken. The result is the differential spectrum described by two power laws with the corresponding spectral indices  $\gamma_1 = \tilde{\gamma}_1 + 1$  and  $\gamma_2 = \tilde{\gamma}_2 + 1$ . It is assumed that all free parameters of equations (1) and (2) are time dependent during the event, that is,  $R_0 \equiv R_0(t)$ ,  $J_0 \equiv J_0(t)$ , etc. In the following, results obtained using equation (1) are labeled as *power law*, and results obtained using equation (2) are labeled as *double power law*.

Using the 1-hr integrated data from HEPAD and EPEAD the parameters of the two functions were derived by fitting the measured GOES-15 data. Both functions were converted to differential energy spectra and fitted to the differential data provided by the instruments; in case of the double power law, the derivative of equation (2) with respect to  $R$  was used. The EPEAD instrument provides a data set for each energy channel of the A and B detector which are oppositely directed and one looking east and one west. The westward looking detector is considered to be more representative for the proton intensity in interplanetary space. Nominally the B detector looks west and the A detector east, but this relationship reverses when the spacecraft is inverted (so-called “yaw flip”; for details see Rodriguez, 2012; Rodriguez et al., 2010). Accordingly, for the analysis in this work the westward facing detector (A for GOES-15) was selected and the corresponding energy calibration provided by Bruno (2017) was used. The differences in the calibration of the A and B detectors, however, are in the percent region only. The lowest and highest energy channels used in this analysis were the EPEAD P3 channel (nominal energy range 9–15 MeV) and the HEPAD P11 channel (nominal energy range  $> 700 \text{ MeV}$ , recalibrated 1094 MeV; Bruno, 2017). As the EPEAD data provided by NOAA are already

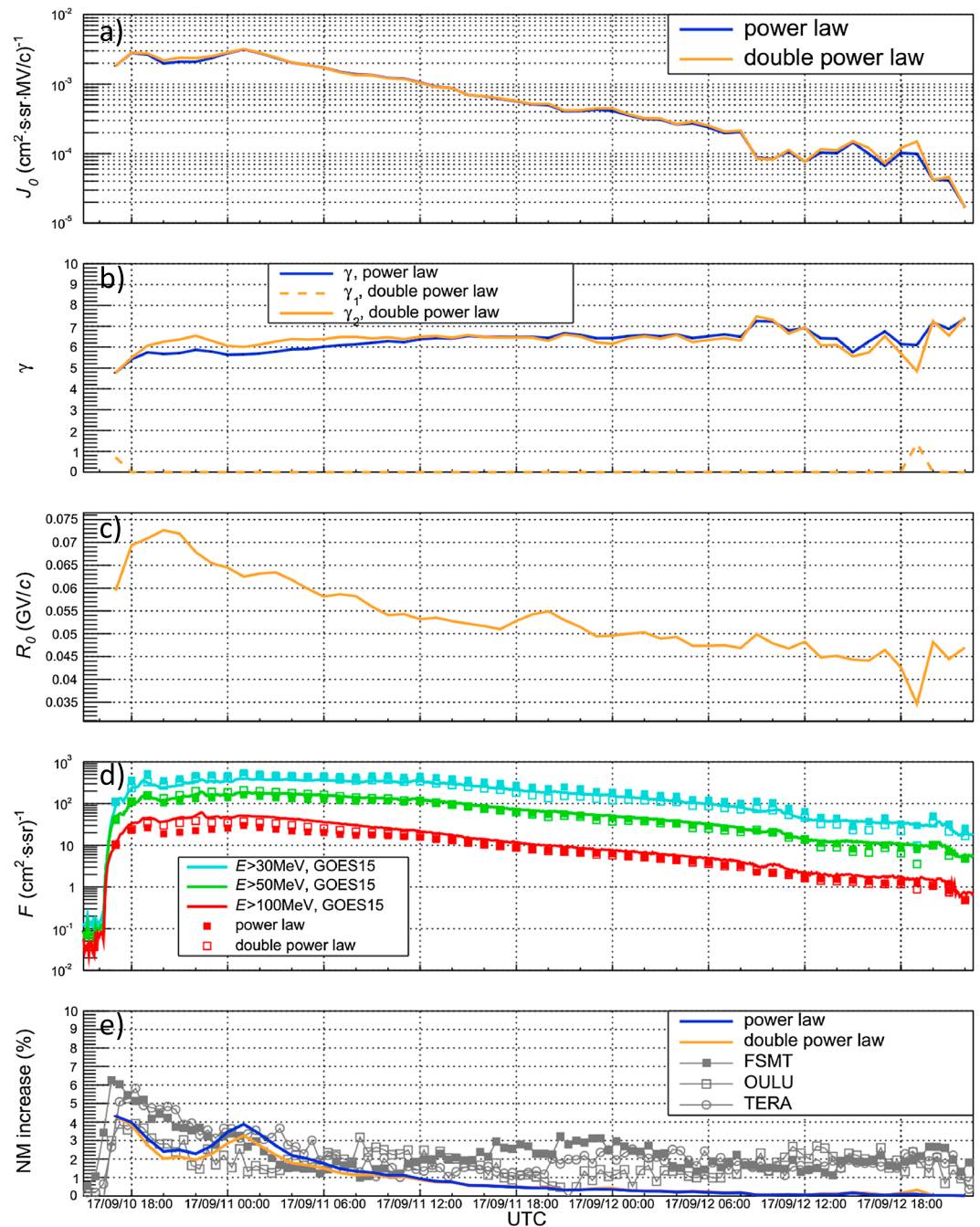


**Figure 2.** (a–c) Results of the parameter fit of the primary spectra during the event; (d) resulting integral proton fluxes in comparison to Geostationary Operational Environmental Satellite-15 measurements; (e) calculated neutron monitor count rate increases compared to measurements of three sea-level stations (Fort Smith-FSMT, Oulu-OULU, and Terre Adelie-TERA).

background corrected, only in the HEPAD data was the background removed using the preevent average between 10 September 2017 00:00 UTC and 16:00 UTC.

Figures 2a–2c show the resulting parameters from fitting the power law and double power law functions to the GOES data. The parameter  $J_0$  shown in Figure 2a is renormalized from equation (2) to the corresponding parameter of the differential spectrum which is the differential proton flux at  $R = 1$  GV/c.  $J_0$  for both functions is almost identical over the whole event. Also, the spectral index of the power law  $\gamma$  and the spectral index  $\gamma_2$

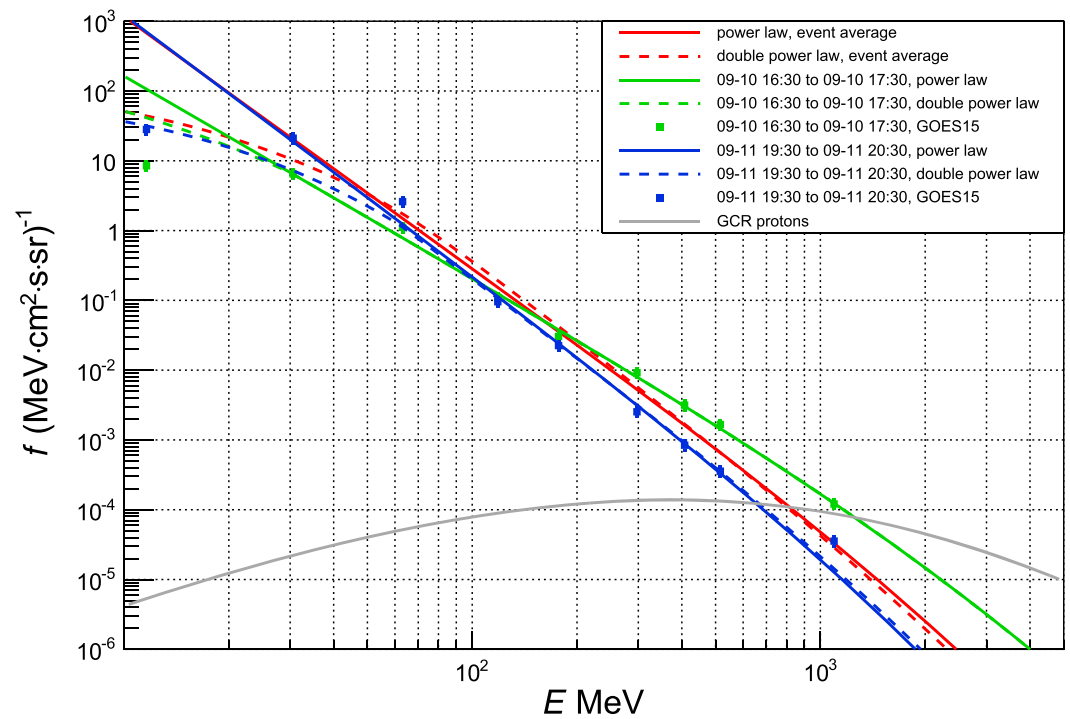


**Figure 3.** Derived proton spectra: Geostationary Operational Environmental Satellite-15 electron, proton, and alpha detector and high-energy proton and alpha detector data and the fit to the data using a power law and a double power law: first hour of the event (green), after 27 hr (blue), and averaged over 54 hr (red). Galactic cosmic radiation proton spectrum is shown for comparison (gray).  $R_0$  for the double power law spectra: 0.059GV ( $\cong$  1.9 MeV) for the first hour and 0.055GV ( $\cong$  1.6 MeV) after 27 hr.

of the high energy part of the double power law are very similar. The derived proton spectra in the first time interval, in the middle of the event, and average over the whole analyzed time period are illustrated in Figure 3.

In order to cross-check the result of the fit, the integral proton flux above 30, 50, and 100 MeV calculated from the power law and double power law spectra are compared to the GOES measurements in Figure 2d. The figure shows that the agreement is good and that the results from the two functions are very similar.

As the data measured by the GOES HEPAD only give information up to energies of around 1 GeV, it is important to validate the extrapolation if one is interested in higher energies. Energies above 1 GeV are of importance for the radiation field at aviation altitudes as the contribution of lower energies is reduced by the substantial shielding provided by the residual atmosphere. In order to validate the extrapolated energy spectrum, the derived energy spectra were used to calculate the expected neutron monitor count rate increase and the result was compared to measurements of several sea-level stations. The neutron monitor count rate increases were calculated by folding the primary proton spectra during the event and the background GCR spectra with the corresponding yield functions (Matthiä et al., 2009). The analysis of the neutron monitor count rates was complicated by the fact that the event occurred during the recovery phase of the Forbush decrease of an earlier event, which led to a maximum decrease of GCR count rates on the order of 10%. As a consequence, the count rate from GCR was increasing at the time of the event on 10 September 2017 which counteracted the decrease in count rates from the decreasing SEP intensity following its peak intensity. Figure 2e illustrates the calculated count rate increases and the measurements from the Fort Smith (FSMT at 60.02°N, 111.93°W), Oulu (OULU at 65.05°N, 25.47°E), and Terre Adelie (TERA at 66.65°S, 140°E) stations. These stations are close to sea level and at low cut-off rigidities, which means that they do not encounter relevant shielding by the Earth's magnetosphere. The neutron monitor count rates were normalized to the preevent count rate between 10 September 2017 00:00 UTC and 16:00 UTC. It should be noted, however, that the count rates in this time period increased by about 2% due to the aforementioned recovery from the Forbush decrease.



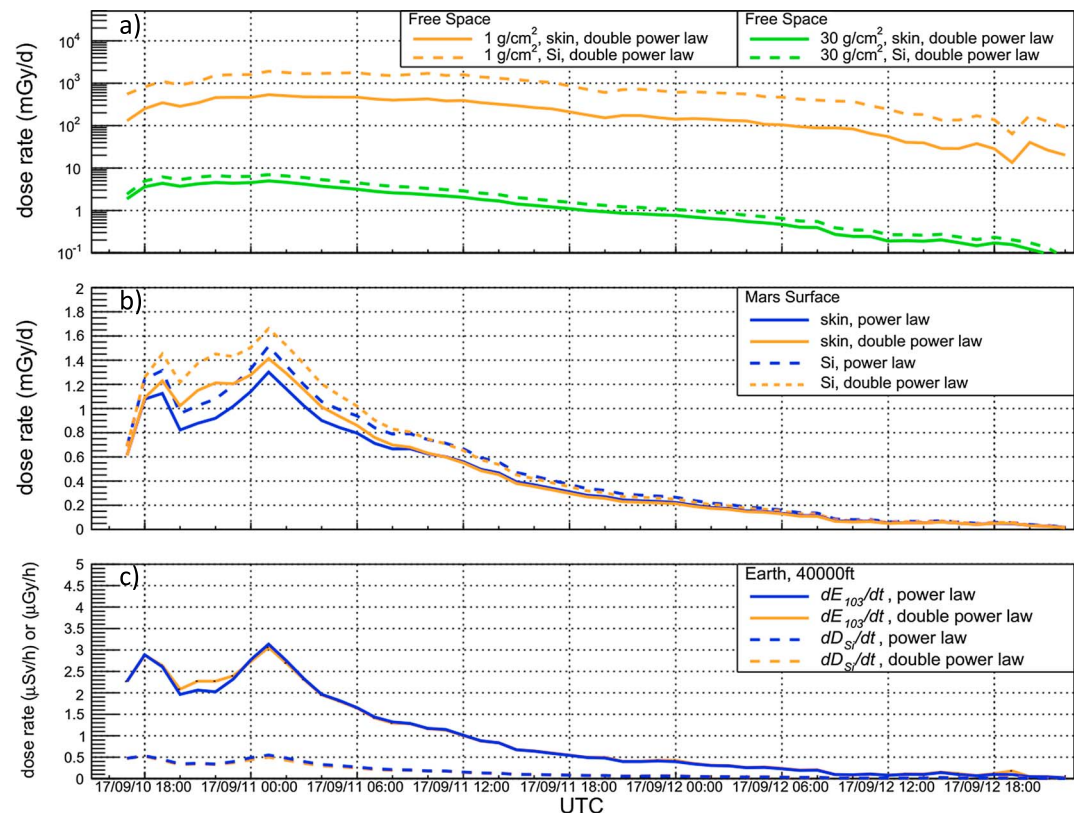


**Figure 4.** Dose rates during the event calculated with the derived proton spectra for three different scenarios: (a) interplanetary space, (b) surface of Mars, and (c) Earth atmosphere at high latitude and high altitude.

Shortly after the onset of the event, the increase caused by the SEP was assumed to be the dominating effect on the count rates. At these times, measured count rate increases of sea level stations at high latitudes were between 4% and 6% with respect to the preevent background (Figure 2e). The count rate increases calculated with the derived primary proton spectra were 4% for both power law and double power law. In the following hours, the calculated count rate increases dropped to about 2% and reached another peak of again 4% shortly after 00:00 UTC on 11 September. The first peak can be attributed to the relatively hard spectrum with  $\gamma$  between 4 and 5 (Figure 2b), which led to larger number of high-energy protons above 1 GeV (Figure 3). Later, the spectrum became softer ( $\gamma$  between 5 and 6), but the integral particle flux reached its maximum after 00:00 UTC on 11 September (Figure 1a). It is impossible to say if this prediction of a second peak is confirmed by the neutron monitor measurements as these also experience diurnal variations in the GCR background count rate that can easily reach 1% to 2% and where the minimum is typically reached around midnight. Altogether, the predicted neutron monitor count rate increases are well within the variation of the measurements of the different stations which gives confidence in the extrapolation of the energy spectrum above 500 MeV.

### 3. Calculated Radiation Exposures During the Event

To estimate the impact of the SEP event on the radiation exposure, dose rates for several scenarios were calculated: (1) interplanetary space, using different amounts of spherical shielding; (2) ISS; (3) Mars surface; and (4) a high-altitude and high-latitude position in the Earth atmosphere.

#### 3.1. Interplanetary Space

To estimate the dose rates and accumulated doses that would have been encountered in interplanetary space during the event, the above derived spectra have been used as primary input spectra to GEANT4 simulations using a spherical shielding geometry. The shielding consisted of an aluminum sphere with an inner radius of

**Table 1***Event Integrated Dose Values Calculated for Interplanetary Space, Mars Surface, and Aviation Altitudes*

			Interplanetary space		Mars surface	Aviation integrated over first 10 hr		
			1 g/cm <sup>2</sup>	30 g/cm <sup>2</sup>				40,000 ft
Power law	Si	mGy	6,136.0	4.7	1.1	Si	μGy	4.4
	Skin	mGy	1,070.0	3.5	1.0	<i>E</i> (ICRP103)	μSv	24.8
	Skin	mSv	3,128.0	8.7	2.2			
Double power law	Si	mGy	1,622	5.3	1.2	Si	μGy	4.1
	Skin	mGy	419.5	3.7	1.0	<i>E</i> (ICRP103)	μSv	25.5
	Skin	mSv	917.6	8.3	2.3			

*Note.* For interplanetary space and Mars, the dose rates were integrated between 10 September 2017 16:30 UTC and 12 September 2017 22:30 UTC for a silicon slab (Si) and for the skin dose using the ICRP 123 (ICRP, 2013) conversion coefficients. For aviation the integration was restricted to the first 10 hr of the event. *E* is the effective dose after ICRP 103 (ICRP, 2007).

200 cm and a thickness corresponding to 1 g/cm<sup>2</sup> (0.37 cm) and 30 g/cm<sup>2</sup> (11.1 cm) similar to Matthiä et al. (2013). Particle fluxes inside this spherical geometry were used to calculate dose rates by applying fluence-to-dose conversion coefficients for a silicon detector with 300-μm thickness and human organs. The conversion coefficients for the silicon detector were calculated with GEANT4, and the conversion coefficients for human organs were taken from ICRP 123 (ICRP, 2013). The resulting dose rates for the period between 11 September 2017 16:30 UTC and 12 September 2017 22:30 UTC are illustrated in Figure 4a, and event integrated doses and dose equivalents are given in Table 1. Dose rates in Figure 4a are based on the double power law spectra which more accurately describe the lower energy region in the primary proton spectra. A striking feature of the calculated values is the discrepancy between the dose rate in silicon, which is calculated for a thin layer of material, and the dose rate calculated for human skin, especially for the 1-g/cm<sup>2</sup> shielding. The reasons for these discrepancies are the self-shielding provided by the human body and the secondary particles created in the interaction of the primary protons with the spacecraft. While the silicon slab is taken as unshielded within the aluminum sphere, a given patch of skin is significantly shielded at least for one side by the body. For a steep energy spectrum with a large fraction of low energy protons this can lead to a large discrepancy in the dose rate in small volumes compared to human organs. This effect is more pronounced in the results using the power law description of the spectrum (Table 1).

Additionally, the interaction of the primary protons can lead to a large flux of secondary charged particles, mostly electrons with low range which stop and deposit their energies in very small volumes. For larger volumes this does not lead to a significant increase in the dose as the energy deposition is small compared to the volume mass. For relatively small volumes like the 300-μm Si detector, however, the contribution can be significant. These effects lead to event integrated doses in the simulated silicon detector (1.6 Gy) which are about a factor of four greater than the calculated skin dose (0.42 Gy) for the double power law description. When interpreting these results, it should be kept in mind that a single plane detector in a sphere is not necessarily a realistic description. In reality such a detector would be surrounded by housing, electronics, other detectors, etc. which would have certainly an impact on the radiation field. Nevertheless, the calculation shows that measurements with such a detector are not necessarily sufficient to estimate quantities that are relevant for radiological protection, such as the dose to skin, without further knowledge about the radiation field.

While measurements indicate that the 30-day dose limit to the skin, 1.5 Gy-Eq (NASA, 2014), would have been approached during the event on the lunar surface for a lightly shielded environment (Schwadron et al., 2018), the calculation presented in this work suggests that the self-shielding of the body alone would have been sufficient to reduce the dose to the skin well below the limit, even in interplanetary space where dose rates are approximately twice as high as on the lunar surface. Schwadron et al. (2018) have derived an event integrated dose of about 0.8–0.9 Gy on the lunar surface from their lowest shielded detector D1D2 of the CRaTER instrument. Taking into account a factor of 0.5 compared to interplanetary space caused by the shielding of the moon, this measurement agrees well with the value of 1.6 Gy estimated here for the 1-g/cm<sup>2</sup> Al shielding using the double power law primary spectrum.

The comparison of the calculated dose rate profile (Figure 4a) with measurements also yields good agreement. Dose rates on the lunar surface as published by Schwadron et al. (2018) for CRaTER's D1D2 detector peaked at 0.5–0.6 Gy/d at around 00:00 UTC on 11 September 2017 and dropped to 0.1–0.3 Gy/d on 12

September 2017 which is compatible to the calculated dose rate in Si taking into account a factor of 2 to convert the lunar dose rate to interplanetary space.

Assuming a shielding of  $30 \text{ g/cm}^2$ , calculations of the dose rate and the dose equivalent rate reveal a drop between 2 (double power law) and 3 (power law) orders of magnitude to levels far below the skin dose limit.

### 3.2. International Space Station

Dose rates and accumulated doses on board the ISS are expected to be significantly lower than in interplanetary space. The Earth blocks a significant part of the sky leading to reduced primary particle intensity (factor of 0.67 for an altitude of 400 km). Additionally, the ISS is well shielded by the Earth magnetic field most of the time. Only during certain orbits, it enters areas where the magnetic shielding is low and energetic protons of a few hundred MeV can reach the station. This behavior was clearly observed for the 10 September event (Berger et al., 2018). The event started at 16:04 UTC on 10 September, but relevant ISS orbits with lower geomagnetic cut-offs allowing the lower energy protons to reach ISS were only passed at around 04:00 on 11 September 2017 with an observed main peak of the event following at 07:30 UTC on 11 September. Higher dose rates were still observed on 12 September 2017 at low  $R_c$  values. The additional dose due to the event measured with relevant silicon detector systems (DOSIS-3D DOSTEL and ISS-RAD) accounted for 68 to  $146 \mu\text{Gy}$ . In Berger et al. (2018) the primary spectra of the protons derived within this work have been used in combination with a model of the Earth's magnetic field and a shielding model of the Columbus module to derive the dose rates along the ISS orbit and the event integrated doses for the 10 September event. Calculated results for this event amount to  $110 \mu\text{Gy}$  in Si which is within the range of the values measured with the silicon detector systems inside the Columbus Laboratory. The total dose accumulated during the event corresponded to about 1 day of exposure to the GCR and less than half a day of the total exposure within Columbus including the contribution of trapped particles.

### 3.3. Mars

The calculations performed here for the surface of Mars have to be considered as a hypothetical scenario and cannot be directly related to measurements performed by the Radiation Assessment Detector of the Mars Science Laboratory (MSL-RAD; Hassler et al., 2012, 2014). The reason is that Mars and Earth were widely separated in the ecliptic plane at the time of the event. The source region of the event and the evolving CME were located between the two planets in terms of heliospheric longitude. Nevertheless, comparing the calculated dose rates with the actual measurements can give some insight into the effect of the event on opposite sides of the CME and the related interplanetary shock.

The dose rates calculated for a silicon layer of 0.3 mm and human skin are illustrated in Figure 4b. Event integrated values for the dose and dose equivalent are given in Table 1. The transport calculations of the primary protons through the Martian atmosphere have been performed in the same way as in Matthiä et al. (2017) and Matthiä and Berger (2017). The resulting particle spectra on the surface of Mars have then been converted to dose or dose equivalent applying the identical conversion coefficients as in the interplanetary space scenario. As in the latter case, the self-shielding of the human body cancels out the lower response of the Si detector to neutrons and the generally lower dose measured by silicon detectors related to the material properties. The effect is much less pronounced than in the interplanetary space scenario with the calculated skin dose being about 15% lower than the dose calculated for the silicon layer.

The onset of the event was measured by MSL-RAD on the surface of Mars on 10 September at around 19:50 UTC (Ehresmann et al., 2018; Zeitlin et al., 2018) about 4 hr after the onset at Earth. The total dose measured with the MSL-RAD B detectors amounts to  $418 \mu\text{Gy}$  in Si for the event (Zeitlin et al., 2018) which is less than twice the daily dose from GCR. Comparing these numbers to the result of this work, which predicts a total dose in Si of 1.1 to  $1.2 \text{ mGy}$  (Table 1) at the Martian surface based on the particle spectra measured at Earth, suggests that the event was much weaker at Mars.

### 3.4. Earth Atmosphere and Aviation

The derived spectra were used to calculate a worst case estimation for the radiation exposure in aviation. Due to the substantial amount of shielding provided by the atmosphere, the increase from the SEPs compared to the GCR background is expected to be much lower compared to interplanetary space. The radiation exposure during the event was calculated by applying the derived spectra to the PANDOCA model (Matthiä et al.,



2014). The dose rates were calculated for high altitude (40,000 ft) and high latitude (cut-off rigidity  $R_c = 0$  GV) position to give an upper limit for the expected dose rates in commercial aviation. Figure 4c illustrates the calculated values for the rate of the effective dose  $E$  (after ICRP, 2007) and the dose rate in silicon. The latter is of interest as many measurements are performed with silicon detectors.

Based on the count rate prior to the event, the effective dose rate and dose rate in silicon from GCR were calculated to be  $7.2 \mu\text{Sv/h}$  and  $2.6 \mu\text{Gy/h}$ , respectively. The calculated values for the event reach peak values for the effective dose rate slightly above  $3 \mu\text{Sv/h}$  and dose rates in silicon of about  $0.5 \mu\text{Gy/h}$ . This corresponds to a maximum increase in the effective dose rate of about 40% and in the dose rate in silicon of about 20%. In their application of the WASAVIES model to the event, Kataoka et al. (2018) have independently estimated a maximum rate of the effective dose of approximately  $3 \mu\text{Sv/h}$  at 12 km ( $\approx 39,000$  ft).

About 24 hr after the beginning of the event, when calculated neutron monitor count rate increases were well below 1%, the effective dose rate was estimated to be about  $0.5 \mu\text{Sv/h}$ , that is, 7% of the effective dose rate from GCR. However, it has to be noted that at that time the recovery from the preceding Forbush decrease had continued and the intensity of the GCR had increased as well. For a worst case scenario we assume a presence of 10 hr at high altitudes and high latitudes during the event. In such a case the total effective dose from SEP is estimated to  $25 \mu\text{Sv}$  (Table 1) which is about 35% of the GCR background ( $72 \mu\text{Sv}$ ). A more detailed analysis of the event in terms of radiation exposure in aviation can be found in Copeland et al. (2018).

#### 4. Summary and Conclusions

The SEP event that began on 10 September 2017 around 16:00 UTC was the strongest event in recent years but a relatively weak GLE, showing not more than a few percent increase in sea level neutron monitor count rates. Although even a weak GLE necessarily increases the radiation exposure during the event in space and at high-altitude and high-latitude positions in the atmosphere, the question remains: To what extent?

The answer depends on the duration of the event, the primary particle spectrum, as well as on the magnetic, atmospheric, and mass shielding at the position of interest. In this work, the 1-hr averaged primary proton spectra during the event have been derived from GOES-15 measurements and the high energy extrapolation has been validated with neutron monitor count rates.

1. For aviation, it was estimated that at high latitudes and high altitudes (40,000 ft) the effective dose rates peaked at  $3 \mu\text{Sv/h}$ , which is about 40% of the background dose rate from GCR. For a 10-hr presence at this position starting with the onset of the event, the accumulated effective dose from solar particles was estimated to be  $25 \mu\text{Sv}$  compared to an effective dose of  $72 \mu\text{Sv}$  from GCR. Estimated dose rates in silicon peaked at  $0.5 \mu\text{Gy/h}$  which is about 20% of the GCR background ( $2.6 \mu\text{Gy}$ ). The lower response of the silicon dose rates compared to the effective dose, 20% against 40%, can be attributed to the relatively larger contribution of secondary neutrons created by the lower energetic solar particles. Silicon detectors are mostly insensitive to neutrons.
2. In the specific orbit of the ISS, the station was protected from the SEPs for about 12 hr after the onset of the event. Only after 04:00 UTC on the 11 September 2017 the ISS entered areas where increased radiation from solar particles was observed. Even so, the exposure to the incoming solar particles is restricted to relatively short passages at high latitudes. The total dose in silicon within the Columbus module numerically estimated in this work was  $110 \mu\text{Gy}$  compared to measurements which ranged between 68 and  $146 \mu\text{Gy}$  (Berger et al., 2018). This corresponds to about 1-day exposure to GCR or about half a day exposure to GCR and trapped particles within Columbus on a regular day.
3. In interplanetary space, where no atmospheric or magnetic shielding exists, the astronaut is protected from the radiation only by the spacecraft or, in case of an extravehicular activity, by the space suit. The results of this work imply that the exposure in a lightly shielded environment in interplanetary space would have accounted for a significant fraction of NASA's 30-day dose limit. For heavier shielding, however, the dose is strongly reduced to values that are 2 to 3 orders of magnitude below the limit.
4. For the hypothetical scenario in which an identical event as measured at Earth would have occurred at Mars, the expected event integrated absorbed doses were calculated as 1.1–1.2 mGy in Si, 1.0 mGy in human skin, and 2.2–2.3 mSv dose equivalent in human skin. The real event, however, was significantly weaker at Mars with measurements showing about 30% of the calculated values.

While the estimated accumulated doses for most scenarios investigated in this work are orders of magnitudes below any dose limit, the accumulated skin dose in a lightly shielded environment ( $1\text{-g/cm}^2$  aluminum) in interplanetary space may have reached some 30% of the corresponding NASA dose limit (NASA, 2014). It was also found that the measurements with a thin silicon detector are not always a good approximation for the human skin dose. Especially in a radiation field dominated by low energy particles, such as in interplanetary space with low shielding, neglecting the self-shielding of the body can lead to overestimation of the skin dose if approximated by doses measured with a silicon detector. In aviation, where the radiation field is dominated by secondary neutrons, the effect is the opposite: Due to their insensitivity to neutrons, silicon detectors would respond with a lower increase compared to whole body quantities such as the effective dose.

## Acknowledgments

Neutron monitor data were provided by the Neutron Monitor Database (nmdb.eu), University of Delaware, Sodankylä Geophysical Observatory and Observatoire de Paris. GOES data were provided by NOAA/SWPC through NCEI (<https://www.ngdc.noaa.gov/stp/satellite/goes/dataaccess.html>). DLR was supported by the DLR grant FuE-Projekt "ISS LIFE" (Programm RF-FuW, Teilprogramm 475). Numerical data used in the figures and tables are provided as supporting information to this article.

## References

- Band, D., Matteson, J., Ford, L., Schaefer, B., Palmer, D., Teegarden, B., et al. (1993). BATSE observations of gamma-ray burst spectra. I—Spectral diversity. *The Astrophysical Journal*, 413, 281–292.
- Berger, T., Matthiä, D., Burmeister, S., Rios, R., Lee, K., Semones, E., et al. (2018). The Solar Particle Event on 10 September 2017 as observed on-board the International Space Station (ISS). *Space Weather*, 16. <https://doi.org/10.1029/2018SW001920>
- Bruno, A. (2017). Calibration of the GOES 13/15 high-energy proton detectors based on the PAMELA solar energetic particle observations. *Space Weather*, 15, 1191–1202. <https://doi.org/10.1002/2017SW001672>
- Copeland, K., Matthiä, D., & Meier, M. M. (2018). Solar cosmic ray dose rate assessments during GLE 72 using MIRA and PANDOCA. *Space Weather*, 16. <https://doi.org/10.1029/2018SW001917>
- Ehresmann, B., Hassler, D. M., Zeitlin, C. J., Guo, J., Wimmer-Schweingruber, R. F., Matthiä, D., et al. (2018). Energetic particle radiation environment observed by RAD on the surface of Mars during the September 2017 event. *Geophysical Research Letters*, 45, 5305–5311. <https://doi.org/10.1029/2018GL077801>
- Hassler, D. M., Zeitlin, C., Wimmer-Schweingruber, R. F., Bottcher, S., Martin, C., Andrews, J., et al. (2012). The radiation assessment detector (RAD) investigation. *Space Science Reviews*, 170(1–4), 503–558. <https://doi.org/10.1007/s11214-012-9913-1>
- Hassler, D. M., Zeitlin, C., Wimmer-Schweingruber, R. F., Ehresmann, B., Rafkin, S., Eigenbrode, J. L., et al. (2014). Mars' surface radiation environment measured with the Mars Science Laboratory's Curiosity rover. *Science*, 343(6169), 1244797. <https://doi.org/10.1126/science.1244797>
- ICRP (2007). The 2007 recommendations of the International Commission on Radiological Protection. *Annals of the ICRP*, 37(2–4), 1–332.
- ICRP (2013). ICRP, 123. Assessment of radiation exposure of astronauts in space. ICRP publication 123. *Annals of the ICRP*, 42(4), 1–339. <https://doi.org/10.1016/j.icrp.2013.05.004>
- Jadrníčková, I., Tateyama, R., Yasuda, N., Kawashima, H., Kurano, M., Uchiyori, Y., et al. (2009). Variation of absorbed doses onboard of ISS Russian Service Module as measured with passive detectors. *Radiation Measurements*, 44(9–10), 901–904. <https://doi.org/10.1016/j.radmeas.2009.10.075>
- Kataoka, R., Sato, T., Miyake, S., Shiota, D., & Kubo, Y. (2018). Radiation Dose Nowcast for the Ground Level Enhancement on 10–11 September 2017. *Space Weather*, 16. <https://doi.org/10.1029/2018SW001874>
- Matthiä, D., & Berger, T. (2017). The radiation environment on the surface of Mars—Numerical calculations of the galactic component with GEANT4/PLANETOCOSMICS. *Life Sciences and Space Research*, 14, 57–63. <https://doi.org/10.1016/j.lssr.2017.03.005>
- Matthiä, D., Berger, T., & Reitz, G. (2013). Organ shielding and doses in low-Earth orbit calculated for spherical and anthropomorphic phantoms. *Advances in Space Research*, 52(3), 528–535. <https://doi.org/10.1016/j.asr.2013.03.025>
- Matthiä, D., Hassler, D. M., de Wet, W., Ehresmann, B., Firan, A., Flores-McLaughlin, J., et al. (2017). The radiation environment on the surface of Mars—Summary of model calculations and comparison to RAD data. *Life Sciences and Space Research*, 14, 18–28. <https://doi.org/10.1016/j.lssr.2017.06.003>
- Matthiä, D., Heber, B., Reitz, G., Meier, M., Sihver, L., Berger, T., & Herbst, K. (2009). Temporal and spatial evolution of the solar energetic particle event on 20 January 2005 and resulting radiation doses in aviation. *Journal of Geophysical Research*, 114, A08104. <https://doi.org/10.1029/2009JA014125>
- Matthiä, D., Meier, M. M., & Reitz, G. (2014). Numerical calculation of the radiation exposure from galactic cosmic rays at aviation altitudes with the PANDOCA core model. *Space Weather*, 12, 161–171. <https://doi.org/10.1002/2013sw001022>
- NASA. (2014). NASA Space Flight human-system standard volume 1, revision A: Crew health.(NASA-STD-3001, VOLUME 1). Retrieved from <https://standards.nasa.gov/standard/nasa/nasa-std-3001-vol-1>
- Redmon, R., Seaton, D., Steenburgh, R., He, J., & Rodriguez, J. (2018). September 2017's geoeffective space weather and impacts to Caribbean radio communications during hurricane response. *Earth and Space Science Open Archive*. <https://doi.org/10.1002/essoar.a530e85443c2d357.102532a29f074aec.1>
- Rodriguez, J. (2012). Note on GOES 13–15 solar protons and yaw flips. Retrieved from <https://ngdc.noaa.gov/stp/satellite/goes/doc/Note%20on%20GOES%2013-15%20Yaw%20Flip.pdf>
- Rodriguez, J., Krossschell, J., & Green, J. (2014). Intercalibration of GOES 8–15 solar proton detectors. *Space Weather*, 12, 92–109. <https://doi.org/10.1002/2013SW000996>
- Rodriguez, J., Onsager, T., & Mazur, J. (2010). The east-west effect in solar proton flux measurements in geostationary orbit: A new GOES capability. *Geophysical Research Letters*, 37, L07109. <https://doi.org/10.1029/2010GL042531>
- Schwadron, N. A., Rahmanifard, F., Wilson, J., Jordan, A. P., Spence, H. E., Joyce, C. J., et al. (2018). Update on the worsening particle radiation environment observed by CReTER and implications for future human deep-space exploration. *Space Weather*, 16, 289–303. <https://doi.org/10.1002/2017SW001803>
- Tylka, A. J., & Dietrich, W. F. (2009). A new and comprehensive analysis of proton spectra in ground-level enhanced (GLE) solar particle events. Paper presented at the 31th International Cosmic Ray Conference.
- Tylka, A. J., Dietrich, W. F., & Atwell, W. (2010). Assessing the space-radiation hazard in ground-level enhanced (GLE) solar particle events. Paper presented at the 2010 Fall AGU Meeting, San Francisco, CA.
- Zeitlin, C., Hassler, D. M., Guo, J., Ehresmann, B., Wimmer-Schweingruber, R. F., Rafkin, S. C. R., et al. (2018). Analysis of the radiation hazard observed by RAD on the surface of Mars during the September 2017 solar particle event. *Geophysical Research Letters*, 45, 5845–5851. <https://doi.org/10.1029/2018GL077760>